

LETTER TO THE EDITOR

Application of the mid-IR radio correlation to the \hat{G} sample and the search for advanced extraterrestrial civilisations[★]

M. A. Garrett^{1,2}

¹ ASTRON, Netherlands Institute for Radio Astronomy, Postbox 2, 7990 AA Dwingeloo, The Netherlands
e-mail: garrett@astron.nl

² Leiden Observatory, Leiden University, PO Box 9513, 2300 RA Leiden, The Netherlands

Received 7 June 2015 / Accepted 11 August 2015

ABSTRACT

Wright et al. (2014, ApJ, 792, 26) have embarked on a search for advanced Kardashev Type III civilisations via the compilation of a sample of sources with extreme mid-IR emission and colours. The aim is to furnish a list of candidate galaxies that might harbour an advanced Kardashev Type III civilisation; in this scenario, the mid-IR emission is then primarily associated with waste heat energy by-products. I apply the mid-IR radio correlation to this Glimpsing Heat from Alien Technology (\hat{G}) sample, a catalogue of 93 candidate galaxies compiled by Griffith et al. (2015, ApJS, 217, 25). I demonstrate that the mid-IR and radio luminosities are correlated for the sample, determining a k-corrected value of $q_{22} = 1.35 \pm 0.42$. By comparison, a similar measurement for 124 galaxies drawn from the First Look Survey (FLS) has $q_{22} = 0.87 \pm 0.27$. The statistically significant difference of the mean value of q_{22} for these two samples, taken together with their more comparable far-IR properties, suggests that the \hat{G} sample shows excessive emission in the mid-IR. The fact that the \hat{G} sample largely follows the mid-IR radio correlation strongly suggests that the vast majority of these sources are associated with galaxies in which natural astrophysical processes are dominant. This simple application of the mid-IR radio correlation can substantially reduce the number of false positives in the \hat{G} catalogue since galaxies occupied by advanced Kardashev Type III civilisations would be expected to exhibit very high values of q . I identify nine outliers in the sample with $q_{22} > 2$ of which at least three have properties that are relatively well explained via standard astrophysical interpretations e.g. dust emission associated with nascent star formation and/or nuclear activity from a heavily obscured AGN. The other outliers have not been studied in any great detail, and are deserving of further observation. I also note that the comparison of resolved mid-IR and radio images of galaxies on sub-galactic (kpc) scales can also be useful in identifying and recognising artificial mid-IR emission from less advanced intermediate Type II/III civilisations. Nevertheless, from the bulk properties of the \hat{G} sample, I conclude that Kardashev Type III civilisations are either very rare or do not exist in the local Universe.

Key words. astrobiology – galaxies: general – galaxies: star formation – radio continuum: galaxies – infrared: general

1. Introduction

In a series of papers, Wright et al. (2014a) and Wright et al. (2014b) have presented a detailed description of our current ability to detect the signature of advanced Kardashev Type III civilisations (Kardashev 1964) via the prominent waste heat signature they are expected to produce. Type III civilisations are defined by Kardashev (1964) as those capable of harnessing the stellar energy supply of a galaxy ($\sim 10^{38}$ Watts). Indeed previous studies (e.g. Carrigan 2009), suggest that constructs such as Dyson spheres (Dyson 1960) will radiate most of their waste heat energy at mid-IR wavelengths, corresponding to temperatures of ~ 100 – 600 K.

Wright et al. have embarked on a novel project called Glimpsing Heat from Alien Technology (\hat{G}) based on the results of an all-sky mid-IR survey conducted by the WISE mission (Wright et al. 2010). In particular, Griffith et al. (2015) have recently produced a list of 93 sources (from an original sample of 100 000 resolved WISE detections) that exhibit both extreme mid-IR emission and mid-IR colours. If the radiation measured by WISE is interpreted as waste heat emission from an advanced civilisation, the source sample includes galaxies

reprocessing more than 25% of their starlight into the mid-IR (i.e. $\gamma > 0.25$ in the formalism of Wright et al. 2014b). While some of these sources are well known (e.g. Arp 220), the majority have not been individually studied in any great detail. One significant problem with the \hat{G} approach is the large number of false positives expected in the sample; in particular, there are many ways in which emission in the mid-IR can arise via natural astrophysical processes, e.g. the reprocessing of starlight or active galactic nucleus (AGN) radiation by dust.

One way of identifying bona fide Type III civilisations is to identify outliers in well-determined scaling laws for galaxies, e.g. the Tully-Fisher relation Annis (1999). I argue here, that the infrared radio correlation can also be used in a similar way. The original infrared radio correlation is a fundamental relation for galaxies (van der kruit 1971; Helou et al. 1985; Condon 1992; Yun et al. 2001), covering at least 5 orders of magnitude in luminosity, holding over a wide range of different redshifts, and extending well into the far-IR/mid-IR, and submillimetre domains (Carilli & Yun 1999; Garrett 2002; Elbaz et al. 2002; Ivison et al. 2002; Appleton et al. 2004). Studies of the correlation usually quote q , the logarithm of the ratio of the IR to radio flux densities (luminosities), the latter typically being measured at 1.4 GHz ($\lambda 20$ cm). K-corrected values of q vary from ~ 2.3 in the far-IR

[★] Table 1 is available in electronic form at <http://www.aanda.org>

(60–100 micron) to ~ 1 in the mid-IR (24 micron), and reflect the evolution of the bolometric spectral energy distribution (SED) of a galaxy across the radio, near-IR, mid-IR, and far-IR domains. The correlation is strongest for star forming galaxies, but also applies to many other galaxy types, including radio quiet AGNs (Roy et al. 1998).

The physical explanation for the strength of the correlation is that both the non-thermal radio emission and the thermal IR emission are related to mechanisms driven by massive star formation. For galaxies in which the bulk of the mid-IR emission is associated with waste heat processes, there is no obvious reason why artificial radio emission would be similarly enhanced. While the continuum radio emission level might increase through the use of advanced communication systems, the amount of waste energy deposited in the radio domain is likely to be many orders of magnitude smaller than that expected at mid-IR wavelengths. As a consequence, I propose to apply the mid-IR radio correlation to the 93 \hat{G} sources presented in Table 9 of Griffith et al. 2015. In particular, galaxies that are associated with Type III civilisations should appear as outliers in the mid-IR radio correlation with extremely high values of q . It should be noted that this deviation is opposite in sense to other frequent outliers, i.e. radio-loud AGN with systematically low values of q .

In this paper, I calculate values of q for the \hat{G} sample, identifying interesting outliers that are deserving of further study. In Sect. 2 I introduce details of the sample and the auxiliary radio and IR data. Section 3 presents the main results, and these are discussed further in Sect. 4. Section 5 presents the main conclusions of the paper with a suggestion for further work.

2. The \hat{G} sample and auxiliary data

Griffith et al. (2015) have identified $\sim 100\,000$ resolved sources detected by WISE, and located above the galactic plane ($b > 10^\circ$). By avoiding the Milky Way and similarly dense regions of the sky such as the LMC, and by applying various colour criteria, Griffith et al. (2015) eliminate confounding objects such as galactic stars, diffuse nebular emission, and other stellar artefacts. The resulting cleaned catalogue of $\sim 31\,000$ extended red objects is therefore biased to include nearby galaxies that are prominent mid-IR sources with extreme colours. In addition, Griffith et al. (2015) apply the AGENT methodology (Wright et al. 2014b) to identify 93 sources that have mid-IR colours consistent with $\gamma > 0.25$ where γ is the fraction of starlight re-emitted in the mid-IR as waste heat products, as modelled by the Wright et al. (2014b) AGENT analysis of the four WISE observing bands (3.4, 4.6, 12, and 22 microns).

I have cross-matched the \hat{G} sample of 93 sources (see Griffith et al. 2015, Table 9) with the NRAO/VLA Sky Survey (NVSS) 1.4 GHz (20 cm) radio catalogue (Condon et al. 1998). I have restricted our study to the 92 sources that fall within the NVSS survey area and have measured redshifts. Since the sources are all resolved by WISE, they are mostly local systems with the median redshift being 0.028. The highest redshift source in the sample has $z = 0.14525$. I compare the $\lambda 20$ cm radio emission with the WISE (band 4) 22 micron data since for local galaxies this band is dominated by continuum emission. The remaining WISE bands are more sensitive to polycyclic aromatic hydrocarbon (PAH) spectral features. Redshifts for the sources, together with IRAS 60 and 100 micron flux densities (where available), were extracted from a search of the NASA/IPAC Extragalactic Database (NED) and SIMBAD. The WISE magnitude system

was converted to Jansky following Wright et al. (2010). The main data are presented in Table 1.

3. Determining k-corrected values of q for the \hat{G} subsample

Following Appleton et al. (2004) I define $q_{22} = \log(S_{22\mu}/S_{20\text{cm}})$ where $S_{22\mu}$ and $S_{20\text{cm}}$ are the source flux densities measured by WISE and NVSS at wavelengths of 22 μm (WISE band 4) and 20 cm. Since the majority of the source samples are typically located in the local universe, the values of q_{22} derived are relatively insensitive to any reasonable k-correction. Nevertheless, a k-correction has been applied to the analysis presented here to ensure consistency with other authors' results obtained for higher- z samples. For the radio, I adopt a k-correction factor of $(1+z)^{+0.7}$ following Appleton et al. (2004). For the mid-IR corrections, and in particular q_{22} , I assume an M82-like SED as presented in Sturm et al. (2000). Over the limited redshift range associated with the \hat{G} sample (22–26 μm), the k-correction is also well modelled by a power-law: $(1+z)^{-2.45}$.

Figure 1 presents a plot of the k-corrected 22 μm mid-IR luminosity ($L_{22\mu}$, W/Hz) against the 20 cm radio luminosity ($L_{20\text{cm}}$, W/Hz) for the \hat{G} sample (red dots). The data clearly show a strong correlation between the mid-IR and radio luminosities. A formal fit to the observed correlation yields

$$\log(L_{22\mu}) = (0.76 \pm 0.09) \log(L_{20\text{cm}}) + (6.65 \pm 0.37).$$

For a subset of the \hat{G} sample (37 of the 92 sources) identified by Griffith et al. (2015) as galaxies (so excluding AGN, Sy 1 & 2, etc.) I similarly find

$$\log(L_{22\mu}) = (0.79 \pm 0.15) \log(L_{20\text{cm}}) + (6.08 \pm 0.33).$$

In addition, a k-corrected value of $q_{22} = 1.35 \pm 0.42$ is derived for the full sample. By comparison, a value of $q_{22} = 1.40 \pm 0.34$ is also derived, again for the same subset of 37 sources identified as galaxies. Table 1 presents the values of q derived for the full source sample, including upper limits for the ten sources that are below the 2.5 mJy detection threshold of NVSS. The table is presented in order of decreasing q_{22} .

As far as I can ascertain, q_{22} has not yet been derived for any other source samples observed by WISE. Appleton et al. (2004) derived a zero-redshift value for $q_{24} = 0.84 \pm 0.28$ for a source sample derived from *Spitzer* observations of the First Look Survey (FLS). In Fig. 1 I also present the data for the \hat{G} sample together with a k-corrected plot of $L_{22\mu}$ vs. $L_{20\text{cm}}$ (W/Hz) for 124 galaxies located in the FLS that I also identify in the WISE all-sky catalogue with sources of known redshift, such that $z < 0.2$ (Marleau et al. 2007). As expected, the FLS sample (plotted as triangles) clearly shows a strong correlation between the mid-IR and radio luminosities with a spread that is smaller than the \hat{G} galaxy sample. The slope of the best linear fit to the FLS data is similar to that seen in the \hat{G} subsample. A formal fit to the observed correlation in the FLS galaxy sample yields

$$\log(L_{22\mu}) = (0.70 \pm 0.07) \log(L_{20\text{cm}}) + (7.36 \pm 0.22).$$

I derive a k-corrected $q_{22} = 0.87 \pm 0.27$ for this FLS subsample. Considering the small wavelength difference, this is plainly consistent with the values of q_{24} derived by Appleton et al. (2004).

Inspection by eye of Fig. 1, suggests that the mean difference between the \hat{G} and FLS samples ($q_{22} = 1.35 \pm 0.42$ vs. $q_{22} = 0.87 \pm 0.27$) may be significant. Indeed, applying Student's

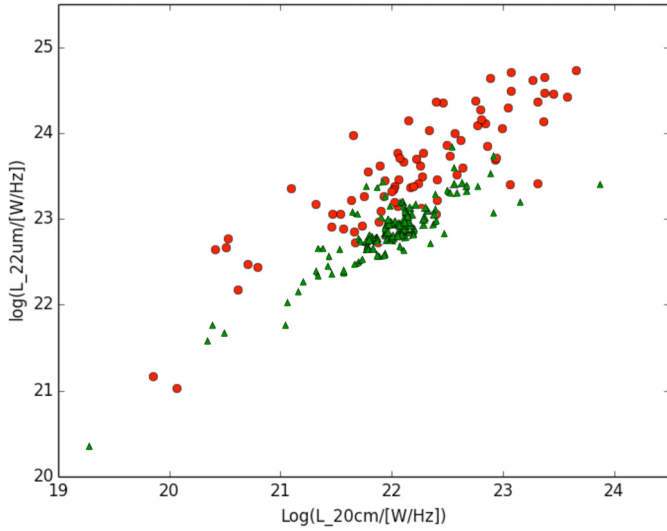


Fig. 1. k-corrected $22\ \mu$ mid-IR luminosity ($L_{22\ \mu}$, W/Hz), plotted against the 20 cm radio luminosity ($L_{20\ \text{cm}}$, W/Hz) for the \hat{G} (red circles) and FLS (green triangles) samples.

T-test (Student 1908) to the data shows the difference between the means (0.48) to be statistically significant at the 95% confidence level (with the two-tailed P value < 0.0001 , $t(204) = 9.99$, a pooled variance of 0.45, and a 95% confidence interval of the mean difference ranging between lower and upper limits of 0.3852 to 0.5748).

The value of q_{FIR} was also determined for a subset of the \hat{G} sample (with both 60 and 100 micron flux densities) finding $q_{\text{FIR}} = 2.45 \pm 0.39$. This is consistent with values found in much larger local galaxy samples, e.g. $q_{\text{FIR}} = 2.34 \pm 0.1$ (Yun et al. 2001).

Systematic underestimates of the radio flux density do not seem to be a major factor in our analysis, despite the extended nature of the sources, and the limited uv-coverage afforded by the NVSS snapshot observations. In particular, the fitted sizes of the sources are typically less than the NVSS synthesised beam (i.e. < 45 arcsec). I conclude that the higher value of q for the \hat{G} subsample is a physical characteristic of the source sample, and this has its origins in enhanced mid-IR emission rather than some systematic radio deficit.

Figure 2 presents a plot of q_{22} against the $22\ \mu$ mid-IR luminosity ($L_{22\ \mu}$, W/Hz) of the \hat{G} sample. Outlying sources with $q_{22} > 2$ are positioned above the dashed line. Details of the same sources are also presented towards the top of Table 1.

4. Discussion

Both the mid-IR and radio luminosities of sources in the \hat{G} subsample are strongly correlated with each other. This clearly demonstrates that the source sample as a whole follows the well-established mid-IR radio correlation associated with natural astrophysical processes such as massive star formation. One interesting, though perhaps not unexpected feature of the \hat{G} sample is that the mean value of q_{22} appears to be statistically different and indeed larger than that determined for the FLS sample. The fact that the values of q_{FIR} are comparable between the samples suggests that this probably reflects a systematic excess in mid-IR emission associated with the \hat{G} sample rather than a deficit of the sample in the radio domain.

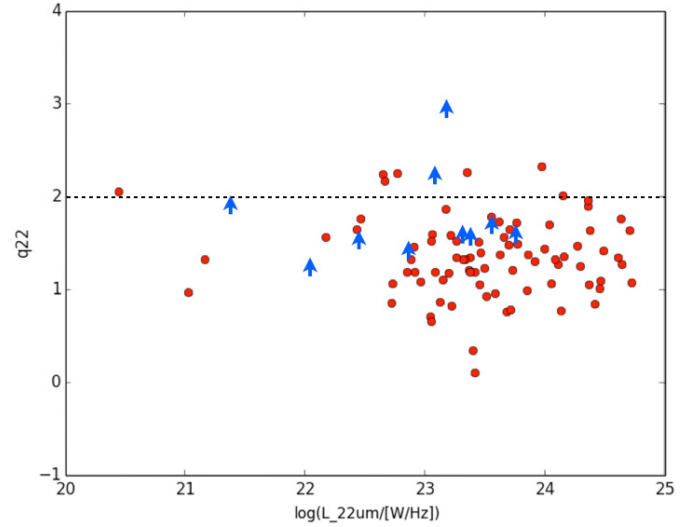


Fig. 2. k-corrected values of q_{22} plotted against the $22\ \mu$ mid-IR luminosity ($L_{22\ \mu}$, W/Hz) for the \hat{G} sample (red filled circles). Above the dashed line, lie the 9 outliers from the sample with $q_{22} > 2$. Sources not detected in the NVSS radio survey show lower limits for q_{22} , and are presented as arrows.

High values of q_{22} would be expected for systems dominated by Kardashev Type III civilisations, and this makes the outliers in the \hat{G} sample of particular interest. Sources with $q_{22} > 2$ (i.e. those lying $> 1.5\sigma$ from the \hat{G} sample mean or $> 4\sigma$ from the FLS sample mean) include MCG+02-60-017, IC 342, ESO 400-28, NGC 814, NGC 4747, NGC 5253, UGC 3097, NGC 4355, and NGC 1377. Astrophysical explanations for high values of q in the mid-IR include (i) very young star forming systems in which the synchrotron radio component is not fully established or (ii) obscured AGNs that heat nuclear dust to relatively warm temperatures. Of the sources with $q_{22} > 2$ presented here, NGC 1377, NGC 4355, and IC 342 have been studied in some depth. Altao et al. (2012) favour an interpretation for NGC 1377 in which the prominent molecular outflow is driven by a young AGN embedded in a dust enshrouded nucleus. By comparison, IC 342 is a nearby face-on barred spiral galaxy with a central nuclear starburst, fed by bar-driven gas inflow (Schinnerer et al. 2003). The compact nucleus of NGC 4355 (also known as NGC 4418) also harbours an extremely rich and dusty molecular environment, but it is unclear whether a compact starburst or an AGN (or some combination of both) power the strong mid-IR component (Varenius et al. 2014). These three examples are probably typical representations of the range of types that dominate the \hat{G} sample with large values of q_{22} .

5. Conclusions and next steps

In this paper, I have demonstrated that the IR-radio correlation can be employed as a useful diagnostic in distinguishing between mid-IR emission produced by natural astrophysical processes and that generated by artificial means, e.g. the waste heat energy associated with Type III civilisations. In particular, galaxies dominated by Type III civilisations should present themselves as extreme outliers to the mid-IR radio correlation with values of $q_{22} > 2$. In this way, the mid-IR radio correlation can be used to eliminate false positives from the \hat{G} sample, and to identify those systems that deserve further detailed study.

The observations presented here demonstrate that the \hat{G} sample of 93 sources (Griffith et al. 2015, Table 9) typically follow the IR-radio correlation. I suggest that the vast majority, if not all of these sources present mid-IR emission associated with natural astrophysical processes. Those sources with $q_{22} > 2$ that have not yet been widely studied in the literature deserve further investigation, however. Nevertheless, from the bulk properties of the \hat{G} sample presented here, I conclude that these sources do not obviously harbour Kardashev Type III civilisations, and that therefore such civilisations are either extremely rare or do not exist in the local universe.

Finally, it should be noted that the IR-radio correlation is also known to hold on sub-galactic scales (e.g. Murphy 2006). A comparison of resolved mid-IR and radio images of nearby galaxies on kpc scales can also be useful in identifying artificial mid-IR emission from advanced civilisations that lie between the Types II and III. While Wright et al. (2014a) venture that Type III civilisations should emerge rapidly from Type IIs, it might be that some specific galactic localities are preferred (see e.g. Cirkovic & Bradbury 2006) or are to be best avoided, e.g. the galactic centre. A comparison of the resolved radio and mid-IR structures can therefore also be relevant to future searches of waste heat associated with advanced civilisations.

Acknowledgements. Part of this work was supported by an IBM Faculty Award. This research has made use of the NASA/IPAC Extragalactic Database (NED) which is operated by the Jet Propulsion Laboratory, California Institute of Technology, under contract with National Aeronautics and Space Administration. This research has made use of the SIMBAD database, operated at CDS, Strasbourg, France. This research has made use of the NASA/IPAC Infrared Science Archive, which is operated by the Jet Propulsion Laboratory, California Institute of Technology, under contract with the National Aeronautics

and Space Administration. I would like to thank the anonymous referee for very helpful and constructive comments, these helped to strengthen and improve the final version of this paper.

References

- Altao, S., Muller, S., Sakamoto, K., et al. 2012, *A&A*, 546, A68
 Annis, J., 1999, *J. British Interplanet. Soc.*, 52, 33
 Appleton, P. N., Fadda, D. T., Marleau, F. R., et al. 2004, *ApJS*, 154, 147
 Carilli, C. L., & Yun, M. S. 1999, *ApJ*, 513, 13
 Carrigan, R. A. 2009, *ApJ*, 698, 2075
 Cirkovic, M. M., & Bradbury, R. J. 2006, *New Astron.*, 11, 628
 Condon, J. J. 1992, *ARA&A*, 30, 575
 Condon, J. J., Cotton, W. D., Greisen, E. W., et al. 1998, *AJ*, 115, 1693
 Dyson, F. J. 1960, *Science*, 131, 1667
 Elbaz, D., Cesarsky, C. J., Chantal, P., et al. 2002, *A&A* 384, 848
 Garrett, M. A. 2002, *A&A*, 384, 19
 Griffith, R. L., Wright, J. T., Maldonado, J., et al. 2015, *ApJS*, 217, 25
 Helou, G., Soifer, B. T., & Rowan-Robinson, M. 1985, *ApJ*, 298, L7
 Ivison, R. J., Greve, T. R., Smail, I., et al. 2002, *MNRAS*, 337, 1
 Kardashev, N. S. 1964, *Sov. Astron.*, 8, 217
 Marleau, F. R., Fadda, D., Appleton, P. N., et al. 2007, *ApJ*, 663, 218
 Murphy, E. J., Braun, R., Helou, G., et al., 2006, *ApJ*, 638, 157
 Roy A. L., Norris R. P., Kesteven M. J., Troup E. R., & Reynolds J. E., 1998, *MNRAS*, 301, 1019
 Schinnerer, E., Boker, T., & Meier, D. S. 2003, *ApJ*, 591, L115
 Student. 2008, *Biometrika*, 6, 1
 Sturm, E., Lutz, D., Tran, D., et al. 2000, *A&A*, 358, 481
 van der Kruit, P. C. 1971, *A&A*, 15, 110
 Varenus, E., Conway, J. E., Martí-Vidal, I., et al. 2014, *A&A*, 566, A15
 Wright, E. L., Eisenhardt, P. R. M., Mainzer, A. K., et al. 2010, *AJ*, 140, 1868
 Wright, J. T., Mullan, B. A., Sigurdsson, S., & Povich, M. S. 2014a, *ApJ*, 792, 26
 Wright, J. T., Griffith, R. L., Sigurdsson, S., Povich, M. S., & Mullan, B. A. 2014b, *ApJ*, 792, 27
 Yun, M. S., Reddy, N. A., & Condon, J. J. 2001, *ApJ*, 554, 803

Table 1. The \hat{G} sample studied in this paper, including values (or upper limits) of q_{22} .

RA (J2000)	Dec (J2000)	$S_{20\text{ cm}}$	WISE-4 (mag)	q	z	γ	SIMBAD Type	Name
03 36 39.05	-20 54 06.8	<2.5	1.5	>2.88	0.005921	0.5	GiG	NGC 1377
12 26 54.61	-00 52 39.1	40.8	-0.15	2.326	0.007048	0.85	Sy2	NGC 4355
04 35 48.45	+02 15 29.6	3.9	2.54	2.263	0.012014	0.52	G	UGC 3097
13 39 55.96	-31 38 24.4	84.7	-0.73	2.248	0.001345	0.60	AGN	NGC 5253
12 51 45.54	+25 46 28.5	7.4	1.92	2.244	0.003966	0.53	IG	NGC 4747
02 10 37.63	-15 46 24.2	5.0	2.54	2.164	0.005405	0.54	G	NGC 814
20 28 25.49	-33 04 20.5	<2.5	3.29	>2.156	0.01228	0.32	G	ESO 400-28
03 46 48.35	+68 05 46.5	190.7	-1.12	2.054	7.7e-05	0.49	GiG	IC 342
23 47 09.20	+15 35 48.3	9.2	2.2	2.008	0.026105	0.65	Sy2	MCG+02-60-017
00 36 52.44	-33 33 16.8	26.8	1.17	1.963	0.020558	0.66	AGN	ESO 350-38
22 52 34.71	+24 43 49.4	7.3	2.67	1.9	0.04193	0.60	AGN	Mrk 309
18 16 03.19	+47 37 05.4	3.2	3.74	1.862	0.01706	0.39	G	2MASX J18160312+4737056
10 25 08.18	+17 09 14.1	<2.5	4.14	>1.829	0.002512	0.58	IG	NGC 3239
10 01 25.94	-15 46 12.2	44.0	1.14	1.776	0.007895	0.34	G	NGC 3094
05 55 42.61	+03 23 31.8	32.5	1.52	1.763	0.002669	0.72	H2G	UGCA 116
04 34 00.03	-08 34 44.9	137.1	-0.07	1.756	0.015851	0.63	AGN	NGC 1614
10 38 33.62	-07 10 14.4	66.6	0.8	1.733	0.007283	0.61	G	IC 630
05 43 23.63	+54 00 44.2	6.9	3.24	1.715	0.027019	0.51	G	2MASX J05432362+5400439
13 02 20.39	-15 45 59.0	34.8	1.55	1.702	0.016745	0.53	GiG	MCG-02-33-099 X
05 16 46.24	-12 20 59.4	6.9	3.47	1.651	0.00636	0.26	G	6dFGS gJ051646.2-122100
08 35 38.40	-01 14 07.1	2.7	4.38	1.645	0.0438	0.36	G	2MASX J08353838-0114072
17 38 01.51	+56 13 25.9	5.8	3.51	1.634	0.06519	0.45	Sy2	2MASX J17380143+5613257
20 57 24.32	+17 07 38.5	43.2	1.43	1.632	0.035	0.70	G	IRAS F20550+1655SE
17 34 31.80	+47 13 01.7	<2.5	4.54	>1.621	0.03901	0.29	G	2MASX J17343177+4713010
15 48 13.36	-24 53 09.6	6.9	3.59	1.593	0.0139	0.39	EmG	ESO 515-7
19 46 05.40	+64 08 50.1	5.5	3.84	1.585	0.018786	0.26	G	2MASX J19460544+6408494
05 56 52.46	-05 23 03.8	3.1	4.55	1.564	0.007749	0.26	LSB	2MASX J0556522-052308
23 36 14.11	+02 09 17.9	65.8	1.24	1.559	0.00935	0.49	AGN	NGC 7714
10 54 16.74	-39 40 19.3	5.6	3.98	1.524	0.016611	0.31	G	ESO 318-23
14 28 37.03	-39 48 44.1	<2.5	4.81	>1.521	0.03298	0.28	IG	ESO 326-24
18 25 52.75	+37 52 41.6	<2.5	4.74	>1.52	0.05492	0.32	IR	IRAS 18241+3750
12 09 13.87	+26 52 37.4	2.1	5.0	1.518	0.03447	0.26	G	LEDA 38612
06 43 39.31	-27 12 17.6	7.0	3.74	1.514	0.02353	0.27	GiG	2MASX J06433935-2712180
02 45 06.40	-02 07 27.7	<2.5	4.86	>1.496	0.03656	0.29	G	2MFGC 2186
13 45 47.40	+70 04 45.9	8.3	3.58	1.493	0.032012	0.37	G	2MASX J13454733+7004455
19 57 51.88	-32 21 28.2	13.0	3.15	1.48	0.0239	0.35	EmG	6dFGS gJ195751.9-322128
00 54 04.02	+73 05 05.7	113.8	0.84	1.473	0.015823	0.54	G	MCG+12-02-001
05 01 47.35	-18 10 00.8	<2.5	5.02	>1.463	0.01319	0.30	G	NGC 1739
06 45 40.95	+43 34 07.5	3.3	4.72	1.453	0.01982	0.27	G	2MASX J06454097+4334069
13 20 21.98	-23 32 25.9	8.1	3.71	1.435	0.0448	0.35	EmG	2MASX J13202200-2332256
22 44 58.08	-01 46 00.4	13.3	3.16	1.417	0.06262	0.41	G	2MASX J22445816-0145589
13 15 03.51	+24 37 07.8	30.8	2.45	1.4	0.013049	0.61	Q?	IC 860
02 41 43.24	+45 46 26.6	7.5	3.99	1.372	0.032736	0.38	G	2MASX J02414325+4546272
19 41 12.82	+63 05 42.9	5.0	4.37	1.37	0.05267	0.31	G	2MASX J19411289+6305430
18 52 22.44	-29 36 20.7	16.0	3.18	1.354	0.042355	0.37	EmG	6dFGS gJ185222.4-293621
19 12 27.31	-29 02 35.7	7.3	4.1	1.349	0.025629	0.35	EmG	ESO 459-7
15 18 06.13	+42 44 44.8	50.3	1.96	1.347	0.0405	0.60	LIN	IRAS F15163+4255NW
00 42 50.05	-36 52 43.2	6.7	4.22	1.34	0.02374	0.30	G	6dFGS gJ004250.1-365241
06 32 26.08	-24 32 08.3	<2.5	5.29	>1.34	0.02416	0.30	G	ESO 490-11
15 23 09.66	-39 34 48.2	7.2	4.17	1.327	0.02541	0.34	G	2MASX J15230967-3934481
10 20 50.93	-17 18 59.4	5.2	4.52	1.323	0.0293	0.32	EmG	MCG-03-27-005
03 04 45.12	+07 47 39.2	2.3	5.42	1.321	0.02682	0.27	G	2MASX J03044511+0747394
12 15 39.36	+36 19 35.1	33.7	2.59	1.321	0.000977	0.59	SBG	NGC 4228
02 08 05.42	-29 14 32.7	6.4	4.19	1.321	0.0636	0.41	G	6dFGS gJ020805.4-291433
02 55 59.96	+47 48 19.3	19.0	3.16	1.302	0.031332	0.37	G	MCG+08-06-022
00 18 50.88	-10 22 36.6	42.4	2.37	1.275	0.027	0.52	EmG	MCG-02-01-051
15 34 57.25	+23 30 11.5	326.3	0.19	1.272	0.018116	0.79	SyG	Arp 220
15 02 53.22	+16 55 08.4	18.7	3.4	1.226	0.021223	0.33	rG	NVSS J150253+165507
01 20 02.63	+14 21 42.5	49.8	2.24	1.251	0.031555	0.49	LIN	MCG+02-04-025
00 08 20.57	+40 37 55.9	6.9	4.44	1.211	0.046148	0.54	Sy2	2MASX J00082041+4037560
09 23 38.22	-25 16 34.9	14.4	3.74	1.203	0.0214	0.32	GiP	6dFGS gJ092338.2-251635

Table 1. continued.

RA (J2000)	Dec (J2000)	$S_{20\text{ cm}}$	WISE-4 (mag)	q	z	γ	SIMBAD Type	Name
04 28 51.45	+69 34 47.1	9.3	4.26	1.192	0.016168	0.33	G	2MASX J04285125+6934469
04 47 38.41	-17 26 01.8	11.7	4.02	1.192	0.013299	0.39	G	ESO 552-5
14 07 36.99	+16 01 21.6	4.7	4.98	1.185	0.02768	0.25	G	2MASX J14073693+1601212
09 35 48.86	-29 19 55.6	4.1	5.08	1.185	0.0431	0.32	EmG	ESO 434-13
12 53 24.16	-23 45 45.6	3.1	5.37	1.184	0.0475	0.31	EmG	6dFGS gJ125324.2-234546
18 10 41.37	+25 07 23.2	9.7	4.23	1.178	0.02213	0.38	G	2MASX J18104135+2507238
05 47 38.65	-10 35 52.8	<2.5	5.76	>1.169	0.01154	0.25	G	6dFGS gJ054738.7-103552
05 43 23.63	+54 00 44.2	6.9	4.77	1.103	0.027019	0.56	G	2MASX J05432362+5400439
10 59 18.14	+24 32 34.6	57.0	2.44	1.098	0.042876	0.50	LIN	2XMM J105918.1+243234
09 39 30.15	+06 26 13.0	5.7	5.04	1.082	0.02459	0.25	rG	NVSS J093929+062610?2MAS
13 44 42.10	+55 53 13.3	144.7	1.51	1.072	0.03734	0.55	Sy2	Mrk 273
04 55 10.80	+05 35 12.6	7.5	4.81	1.065	0.01671	0.38	G	2MASX J04551070+0535126
23 26 10.59	-30 31 06.1	10.5	4.29	1.065	0.0641	0.28	EmG	6dFGS gJ232610.6-303106
16 36 00.57	+10 13 40.4	4.1	5.09	1.055	0.14525	0.43	G	2MASX J16360060+1013396
15 00 29.00	-26 26 49.2	37.8	3.08	1.053	0.01751	0.65	H2G	2MASX J15002897-2626487
12 13 46.00	+02 48 40.3	23.3	3.54	1.008	0.0731	0.55	LIN	LEDA 39024
22 54 51.03	+37 42 20.8	3.8	5.49	0.993	0.091137	0.28	G	2MASX J22545096+3742205
02 59 41.29	+25 14 15.0	33.1	3.49	0.969	0.001265	0.54	G	NGC 1156
01 16 07.20	+33 05 21.7	75.4	2.57	0.959	0.016044	0.54	Sy2	NGC 449
05 44 21.56	-13 53 11.9	10.5	4.7	0.932	0.0403	0.31	G	2MASX J05442151-1353116
17 34 29.01	-04 05 41.7	6.2	5.44	0.87	0.0363	0.35	G	6dFGS gJ173428.9-040542
05 15 21.42	-26 28 17.1	20.6	4.25	0.855	0.012809	0.30	EmG	ESO 486-39
12 49 30.16	-11 24 03.4	73.4	2.79	0.842	0.047826	0.59	Sy2	IRAS 12468-1107
16 18 33.99	+13 24 25.9	4.6	5.85	0.818	0.04953	0.28	G	2MASX J16183392+1324253
22 21 49.97	+39 50 24.0	7.8	5.31	0.779	0.069725	0.29	G	2MASX J22215143+3950240
00 34 43.48	-00 02 26.6	57.0	3.25	0.774	0.042529	0.54	Sy2	2MFGC 403
02 56 09.76	-15 39 43.5	10.9	5.04	0.756	0.05877	0.33	G	6dFGS gJ025609.8-153946
11 24 02.72	-28 23 15.4	52.1	3.6	0.711	0.01374	0.43	Sy2	IRAS 11215-2806
11 45 43.59	-11 47 12.6	33.3	4.21	0.655	0.018463	0.29	EmG	6dFGS gJ114543.6-114712
10 50 52.15	+01 09 44.2	32.7	4.94	0.343	0.03952	0.29	GiG	IC 649S
13 08 42.02	-24 22 57.8	474.5	2.72	0.103	0.014	0.50	Sy2	PKS 1306-241